TECHNISCHE UNIVERSITÄT DRESDEN

Feasibility studies for the measurement of polarization of the Z boson in electroweak Zjj production

Bachelor-Arbeit
zur Erlangung des Hochschulgrades
Bachelor of Science
im Bachelor-Studiengang Physik

vorgelegt von

Malte Müller,
geboren am 05.12.2002.

Institut für Kern- und Teilchenphysik
Fakultät Physik
Bereich Mathematik und Naturwissenschaften
Technische Universität Dresden

2024

Eingereicht am 16. Dezember 2024

1. Gutachter:	Dr. Frank Siegert
2. Gutachter:	Prof. Dr. Arno Straessner
Betreuer:	Dr. Philip Sommer

Summary

Abstract

The electroweak (EW) Zjj process is sensitive to vector boson fusion (VBF) and features a cross-section significantly larger than that of the closely related vector boson scattering (VBS) process. This makes Zjj an ideal prototype for developing and benchmarking experimental techniques. This thesis presents a feasibility study evaluating the potential to measure the polarization of the Z-boson in Zjj events using the methodology of angular coefficients. An analytical method is employed to construct polarization templates from simulated data. The feasibility was evaluated by fitting these templates in a maximum likelihood to the same simulated data, scaled to an integrated luminosity of 140 fb^{-1}, equivalent to LHC Run 2. The study demonstrated sensitivity primarily to the angular coefficients A_0, A_2, and A_8 and showed that a differential measurement of the longitudinal polarization fraction as a function of the Z-boson's transverse momentum is feasible in this dataset, with statistical uncertainties below 10% up to 400 GeV.

Kurzdarstellung

Der elektroschwache (EW) Zjj-Prozess ist sensitiv gegenüber der Vektor-Boson-Fusion (VBF) und weist einen deutlich größeren Wirkungsquerschnitt auf als der eng verwandte Prozess der Vektor-Boson-Streuung (VBS). Dies macht Zjj zu einem idealen Prototyp für die Entwicklung und Validierung experimenteller Techniken. Diese Arbeit präsentiert eine Machbarkeitsstudie, die das Potenzial zur Messung der Polarisation des Z-Bosons in Zjj-Ereignissen mittels der Methode der Winkelkoeffizienten bewertet. Eine analytische Methode wird angewendet, um Polarisationstemplates aus simulierten Daten zu erstellen. Die Machbarkeit wird durch einen Maximum-Likelihood-Fit dieser Templates an denselben simulierten Datensatz untersucht, skaliert auf eine integrierte Luminosität von 140 fb^{-1}, entsprechend den Daten von LHC Run 2. Die Studie zeigte eine Sensitivität hauptsächlich gegenüber den Winkelkoeffizienten A_0, A_2 und A_8 und bewies, dass eine differentielle Messung des longitudinalen Polarisationsanteils als Funktion des transversalen Impulses des Z-Bosons mit statistischen Unsicherheiten unter 10 % bis zu 400 GeV in diesem Datensatz möglich ist.

Contents

1 Introduction 1

2 Theory 3
- 2.1 Short summary of the Standard Model . . . 3
- 2.2 Electroweak Zjj production mechanism . . . 4
- 2.3 Polarization of the Z-boson . . . 5

3 Extracting angular coefficients 9
- 3.1 Event selection . . . 9
  - 3.1.1 General lepton and jet requirements . . . 9
  - 3.1.2 Vector Boson Fusion topology requirements . . . 10
  - 3.1.3 Signal Region definition . . . 10
  - 3.1.4 Summary of the event selections . . . 10
- 3.2 Monte-Carlo Sample . . . 11
- 3.3 Method of moments . . . 13
- 3.4 Methodology to build templates . . . 14
- 3.5 Summary . . . 15

4 Results 19
- 4.1 Fitting methodology . . . 19
- 4.2 Feasibility study of a measurement in the fiducial phase space . . . 20
  - 4.2.1 Fitting with templates projected on the $\cos\theta$ axis . . . 20
  - 4.2.2 Fitting with double differential templates . . . 21
  - 4.2.3 Summary . . . 22
- 4.3 Feasibility study of a differential measurement in p_T^Z . . . 23

5 Conclusion 27

Appendix 29
- 1 Polynom shape for different p_T^Z bins . . . 29
- 2 Templates in p_T^Z bins . . . 32

Bibliography 39

1 Introduction

Modern physics includes a vast amount of research fields, each exploring the nature of the universe on dramatically different scales. At the largest scales, cosmology investigates the origins and structures of galaxies and galaxy clusters, dealing with scales as large as the size of the observable universe itself, which spans around 10^{26} m. Conversely, particle physics probes the fundamental particles that constitute matter and their interactions at distances of approximately 10^{-18} m.

The most successful framework for describing these elementary particles and their interactions is the Standard Model of particle physics (SM). Over the last five decades, the SM has provided accurate predictions for various particle and process observations in experiments. A milestone in this framework was achieved with the discovery of the Higgs boson in 2012, a breakthrough made possible at the Large Hadron Collider (LHC), the world's largest and most powerful particle accelerator.

Since its commissioning in 2008, the LHC, with its 27 km long accelerator ring beneath CERN near Geneva, has been at the forefront of modern particle physics. By enabling proton-proton collisions at unprecedented center-of-mass energies up to 13.6 TeV, the LHC offers a unique platform to study well-established phenomena within the SM and search for potential deviations that could hint at new physics beyond the SM.

Among these phenomena, Vector Boson Scattering (VBS) of massive gauge bosons is particularly significant, as it probes the self-interactions of gauge bosons and the breaking of the electroweak (EW) symmetry via the Higgs mechanism. The longitudinal polarization states of the intermediate vector bosons provide especially rich insights into these dynamics. A closely related process, the production of a Z-boson via Vector Boson Fusion (VBF), can be used as a prototype process to develop experimental techniques and benchmark theoretical calculations.

This thesis focuses on measuring the electroweak (EW) Z-boson production associated with two jets (Zjj). This process, established experimentally by the ATLAS collaboration [1], is highly sensitive to the VBF Z production mechanism. The primary goal of this research is to investigate the feasibility of measuring the longitudinal polarization in the EW Zjj process using angular coefficients — a methodology successfully applied by ATLAS for another process [2]. By applying and evaluating this approach within the Zjj context, this study aims to assess its potential for future polarization and interaction dynamics measurements in VBF processes at the LHC.

This thesis is organized as follows. **Chapter 2** provides the theoretical foundation, including a brief overview of the Standard Model, the electroweak (EW) production mechanism of a Z-boson in association with two jets (Zjj) via vector boson fusion (VBF), and the parametrization of Z-boson decays using angular coefficients. It also introduces the concept of longitudinal polarization and the Collin-Soper frame for defining angular observables. **Chapter 3** details the methodology for extracting angular coefficients from Monte Carlo (MC) samples using the method of moments. It describes the construction of templates that serve as pseudo-analytical representations of harmonic polynomials in the presence of lepton selection criteria. **Chapter 4** presents the results of the feasibility study for measuring the longitudinal polarization fraction of the Z-boson. The fitting methodology is explained, and closure tests are performed to validate the approach. The chapter concludes by assessing the potential for a differential measurement of the longitudinal polarization as a function of the Z-boson transverse momentum (p_T^Z). Finally, the thesis concludes with a summary of the key findings and an outlook for future studies in **Chapter 5**.

2 Theory

This chapter outlines the theoretical foundation relevant to the study of polarization in the electroweak (EW) production of Z-bosons in association with two jets (Zjj). It begins with a brief overview of the SM, with emphasis on the EW sector and the role of gauge bosons. Next, the phenomenology of EW Zjj production is introduced, focusing on its VBF characteristics. Finally, the chapter explains how the decay of the Z-Boson can be parametrized using angular coefficients, enabling the extraction of polarization fractions from these coefficients.

2.1 Short summary of the Standard Model

The Standard Model of particle physics (SM) is the cornerstone of modern particle physics, describing the fundamental particles and their interactions within a quantum field theory (QFT) framework. In QFT, particles are described as quantized excitations of fields that follow relativistic field equations. The SM is a Yang-Mills theory, where these fields possess internal symmetries represented by mathematical groups. It is built on the principle of local gauge invariance, ensuring consistency with fundamental symmetries of nature. The symmetry groups governing the SM are:

$$\mathrm{SU}(3)_C \times \mathrm{SU}(2)_L \times \mathrm{U}(1)_Y \tag{2.1}$$

where $\mathrm{SU}(3)_C$ corresponds to the strong interaction and $\mathrm{SU}(2)_L\times$ $\mathrm{U}(1)_Y$ unifies the electromagnetic and weak interactions in the electroweak theory.

The SM contains a whole zoo of particles shown in Fig. 2.1. The particles can be divided into two main categories: fermions and bosons.

Fermions are spin-1/2 particles which constitute matter. There are 12 fermions and their corresponding anti-fermions. They can be further divided into quarks (purple) and leptons (green). Quarks participate in the strong interaction, while leptons do not. The six leptons include three electrically charged particles—the electron (e), muon (μ), and tau (τ)—and three neutral neutrinos, each associated with one of the charged leptons.

Bosons are integer-spin particles that mediate the fundamental forces between matter. While the fermions and their quantum numbers are introduced ad hoc, the gauge bosons follow from the symmetry groups postulated in the SM. The electroweak symmetry, $\mathrm{SU}(2)_L\times$

$U(1)_Y$, leads to 4 gauge-bosons: the massive W^+-, W^-- and Z-boson and the massless photon γ. The $SU(3)_C$, corresponding to the strong interactions, yields eight massless gauge-bosons, the gluons g, that differ in color charges. Finally, the Higgs-boson is a heavy particle associated with the Higgs-mechanism, which explains the mass of all massive particles, particularly the massive gauge-bosons from EW-symmetry via spontaneously breaking said symmetry.

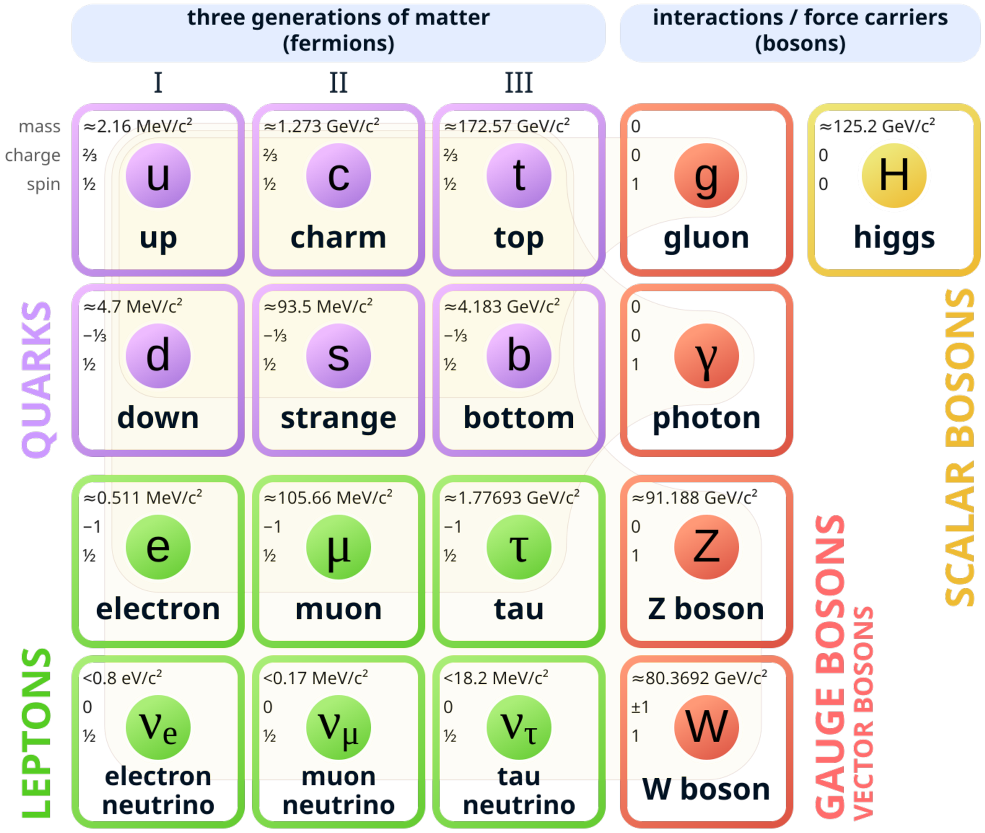

Figure 2.1: The fundamental particles and the mediators of the fundamental interactions that are described in the Standard Model of particle physics [3]

2.2 Electroweak Zjj production mechanism

This investigation centers on the electroweak (EW) production of a Z-boson in association with two jets (Zjj), a process that is sensitive to vector boson fusion (VBF) dynamics and involves interactions amongst the EW gauge bosons. The process is characterized by t-channel exchanges of weak bosons (W, Z, γ), as illustrated in Fig. 2.2 a and b. However, as shown in Fig. 2.2 c and d, the same final state can be produced in mixed strong and electroweak interactions. This will be referred to as the strong Zjj production in the following.

In the purely electroweak production, no colour charge is exchanged between the scattering quarks, leading to a characteristic signature with two high-energy jets in the detector's forward regions. These jets are separated by a large rapidity gap (Δy_{jj}) and exhibit a significant invariant mass (m_{jj}). Accompanying these jets are the decay products of the Z-boson, which, unlike the jets, are produced centrally. This work specifically examines the leptonic decay channels of the Z-boson, namely $Z \to \ell^+\ell^-$, where $\ell = e, \mu$. These characteristics can be used to distinguish the EW Zjj from strong Zjj production by employing kinematic selections.

The purely EW Zjj production has been measured in Ref. [1], providing a foundational understanding of the mechanism. Building on this work, the present thesis aims to explore polarization effects in this process, leveraging the distinct topology and kinematics of vector boson fusion events.

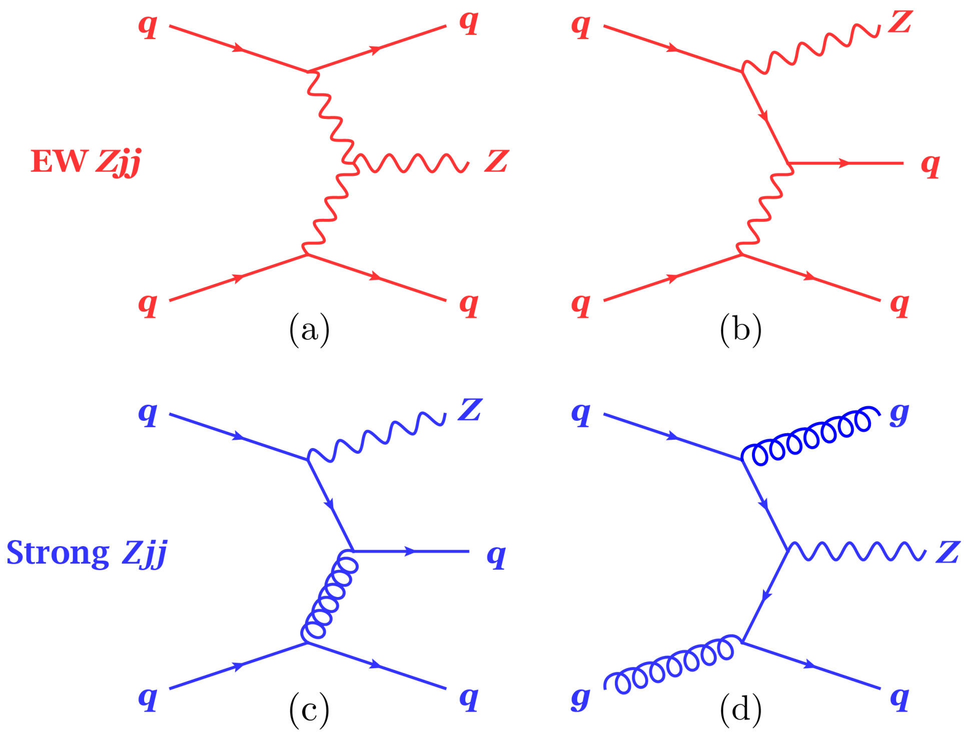

Figure 2.2: Representative Feynman-diagram for electroweak Zjj production (a, b) and strong Zjj production (c, d) [2]

2.3 Polarization of the Z-boson

The Z-boson is a vector boson, which means it has a spin of 1. In quantum mechanics, one can derive that there are $2s+1$ different spin states, where s is the particle's spin. This leads to three polarization states for the Z-boson, two transversally polarized states ($S_Z = \pm 1$) and one longitudinal state ($S_Z = 0$), which can be seen in Fig. 2.3). The longitudinal state is especially interesting since a non-zero longitudinal polarization fraction arises directly from breaking the EW symmetry via the Higgs mechanism.

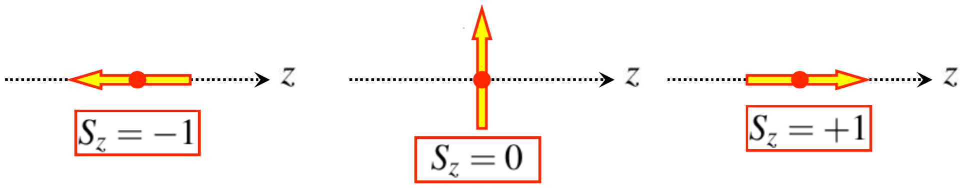

Figure 2.3: Polarization states of vector bosons (Taken from [4])

To extract the longitudinal polarization fraction, the decay dynamics of the Z-boson can be parametrized using nine frame-dependent coefficients. These coefficients are obtained by expanding the differential cross-section into a series of nine harmonic polynomials. The polynomials depend only on the polar and azimuthal decay angles of the leptons, θ and ϕ. To define these angular variables unambiguously, a reference must be chosen. The Collin-Soper frame is used for the feasibility study. It is shown in Fig. 2.4 and defined in the following.

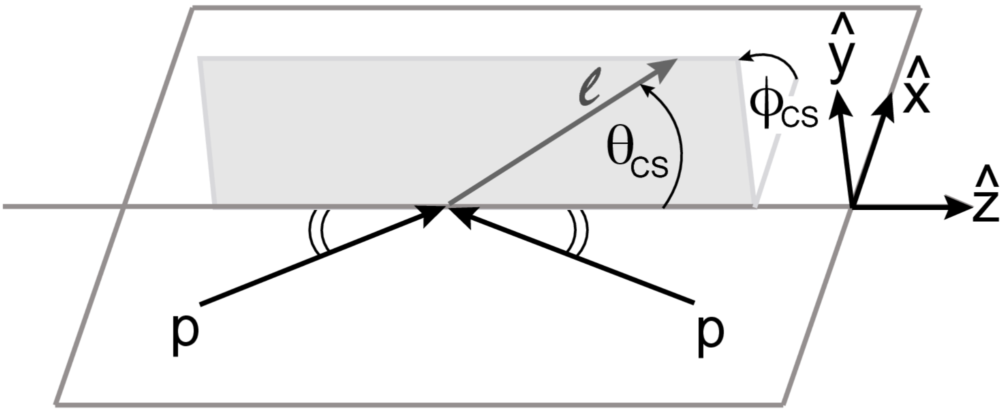

Figure 2.4: Definition of the angles in the Collins-Soper reference frame (Taken from [2])

In the rest-frame of the Z-boson, the z-axis is defined to be the bisector of the incoming proton beams with the positive z direction to be chosen in the direction of the longitudinal momentum of the Z-boson in the laboratory frame. Furthermore, the y-axis is defined by the plane spanned by the two incoming beams and the x-axis so that the coordinate system is right-handed. The polar and azimuthal angles, θ, and ϕ are calculated with respect to the negatively charged lepton.

For the expansion of the differential cross-section of the Z-boson decay, the unpolarized cross-section ($\frac{\mathrm{d}\sigma^{U+L}}{\mathrm{d}p_T^Z \mathrm{d}y^Z \mathrm{d}m^Z}$) is factorized from the angular distribution by convention, resulting in an expression where the coefficients $A_{0-7}(p_T^Z, y^Z, m^Z)$ encapsulate all the information about the shape of the angular distribution of the Z-boson decay. Here, p_T^Z represents the transverse momentum of the Z-boson, y^Z denotes its rapidity (a measure of its velocity along the beam axis), and m^Z refers to its invariant mass.

$$
\begin{aligned}
\frac{\mathrm{d}\sigma}{\mathrm{d}p_T^Z\,\mathrm{d}y^Z\,\mathrm{d}m^Z\,\mathrm{d}\cos\theta\,\mathrm{d}\phi} = \frac{3}{16\pi}\frac{\mathrm{d}\sigma^{U+L}}{\mathrm{d}p_T^Z\,\mathrm{d}y^Z\,\mathrm{d}m^Z}& \\
\{(1+\cos^2\theta) + \frac{1}{2}A_0(1-3\cos^2\theta) + A_1\sin 2\theta\cos\phi& \\
+\frac{1}{2}A_2\sin^2\theta\cos 2\phi + A_3\sin\theta\cos\phi + A_4\cos\theta& \\
+A_5\sin^2\theta\sin 2\phi + A_6\sin 2\theta\sin\phi + A_7\sin\theta\sin\phi\}&
\end{aligned} \tag{2.2}
$$

This provides an analytical expression for the differential cross-section in the full phase space of the Z-boson decay. For this analysis, the coefficient A_0 is especially relevant since the longitudinal polarization fraction f_L^Z of the Z-boson is given by:

$$
f_L^Z = \frac{A_0}{2} \tag{2.3}
$$

The expressions are derived in Ref. [5].

The differential cross section as a function of $\cos\theta$ and ϕ follow from the projection of Eq. 2.2 on the respective variable:

$$
\begin{aligned}
\frac{\mathrm{d}\sigma}{\mathrm{d}p_T^Z\,\mathrm{d}y^Z\,\mathrm{d}m^Z\,\mathrm{d}\phi} &= \int \mathrm{d}\cos\theta\,\frac{\mathrm{d}\sigma}{\mathrm{d}p_T^Z\,\mathrm{d}y^Z\,\mathrm{d}m^Z\,\mathrm{d}\cos\theta\,\mathrm{d}\phi} \\
&= \frac{1}{2\pi}\frac{\mathrm{d}\sigma^{U+L}}{\mathrm{d}p_T^Z\,\mathrm{d}y^Z\,\mathrm{d}m^Z} \\
&\quad \left\{1+\frac{1}{4}A_2\cos 2\phi + \frac{3\pi}{16}A_3\cos\phi + \frac{1}{2}A_5\sin 2\phi + \frac{3\pi}{16}A_7\sin\phi\right\} \qquad (2.4) \\
\frac{\mathrm{d}\sigma}{\mathrm{d}p_T^Z\,\mathrm{d}y^Z\,\mathrm{d}m^Z\,\mathrm{d}\cos\theta} &= \int \mathrm{d}\phi\,\frac{\mathrm{d}\sigma}{\mathrm{d}p_T^Z\,\mathrm{d}y^Z\,\mathrm{d}m^Z\,\mathrm{d}\cos\theta\,\mathrm{d}\phi} \\
&= \frac{3}{8}\frac{\mathrm{d}\sigma^{U+L}}{\mathrm{d}p_T^Z\,\mathrm{d}y^Z\,\mathrm{d}m^Z}\left\{(1+cos\theta) + \frac{1}{2}A_0(1-3\cos^2\theta + A_4\cos\theta)\right\} \qquad (2.5)
\end{aligned}
$$

Both are independent of the coefficients A_1 and A_6.

3 Extracting angular coefficients

This chapter outlines the methodology for extracting the angular coefficients that characterize the Z-boson decay distribution. First, the event selection criteria are defined to isolate the EW Zjj production process. Next, the Monte Carlo sample used for the analysis is introduced. The angular coefficients are then calculated analytically using the method of moments. Finally, templates are constructed to represent the harmonic polynomials in the presence of a selection on lepton kinematics.

3.1 Event selection

The event selection criteria are designed to isolate the electroweak Zjj production process in the vector boson fusion (VBF) topology, which is characterized by a high-energy, large-rapidity-separation dijet system accompanied by a dilepton pair from a Z-boson decay. This selection minimizes background contributions from strong Zjj production. For this analysis, the event selection phase space is chosen to align with the ATLAS collaboration's previous measurement of electroweak Zjj production [1]. Key variables used in the event selection criteria include:

- **Tranverse momentum (p_T)**: A particle's 3-momentum component perpendicular to the beam axis.
- **Pseudorapidity (η)**: Defined as $\eta = -\ln[\tan(\theta/2)]$, where θ is the polar angle. In the ultra-relativistic limit, η approximates the rapidity y
- **Rapidity (y)**: Defined as $y = 0.5\ln[(E + p_z)/(E - p_z)]$, where E is the energy of the particle and p_z is the momentum along the beam axis. This is a measure of the relativistic velocity of the particle along the beam axis.
- **Centrality (ξ_Z)**: Measures the central production of the Z-boson relative to the dijet system, defined as $\xi_Z = |y_{\ell\ell} - 0.5(y_{j_1} + y_{j_2})|/|\Delta y_{jj}|$

3.1.1 General lepton and jet requirements

Events are selected based on the presence of two leptons with the same flavour but opposite charges (e^+e^- or $\mu^+\mu^-$) and at least two jets. Each lepton must satisfy a p_T threshold of $p_T^\ell > 25\,\text{GeV}$. Motivated by the detector geometry of the ATLAS detector, electrons are only used in the analysis if $|\eta| < 2.47$ is satisfied, but excluding the transition region $1.37 < |\eta| < 1.52$. For mouns, the requirement is $|\eta| < 2.4$. The invariant mass of the dilepton system is required to be in the Z-boson mass window ($81\,\text{GeV} < m_{\ell\ell} < 101\,\text{GeV}$). Jets are accepted if they have a minimum transverse momentum of $p_T > 25\,\text{GeV}$. The two leading jets are required to have transverse momenta of $p_T^{j_1} > 85\,\text{GeV}$ and $p_T^{j_2} > 80\,\text{GeV}$, ensuring a high-energy dijet system suitable for probing the VBF topology.

3.1.2 Vector Boson Fusion topology requirements

Additional criteria are imposed on the jet kinematics and event topology to enhance the sensitivity to Zjj production in the VBF topology. The invariant mass of the two leading jets (m_{jj}) is required to exceed $1000\,\text{GeV}$, suppressing low-mass backgrounds from strong Zjj production and focusing on the high-mass region characteristic of VBF events. Furthermore, the rapidity difference between the two leading jets ($|\Delta y_{jj}|$) must satisfy $|\Delta y_{jj}| > 3.0$, exploiting the characteristic rapidity gap in VBF processes.

3.1.3 Signal Region definition

The signal region is further refined with cuts targeting central Z-boson production relative to the dijet system and suppressing additional activity within the rapidity gap. The centrality must satisfy $\xi_Z < 0.5$. This ensures the Z-boson is produced centrally in the rapidity space between the two jets. Additionally, events are required to have no extra jets with $p_T > 25\,\text{GeV}$ within the rapidity interval between the two leading jets, effectively suppressing backgrounds from gluon radiation and other QCD processes.

3.1.4 Summary of the event selections

The previously explained event selection criteria separate the EW Zjj production from backgrounds like the strong Zjj production. A summary of the criteria can be found in Tab. 3.1. Furthermore, the ATLAS collaboration [1] made a standard Rivet [6] analysis available, which is the foundation for my polarization studies.

Dressed muons Dressed electrons Jets	$p_T > 25\,\text{GeV}$ and $\lvert\eta\rvert < 2.4$ $p_T > 25\,\text{GeV}$ and $\lvert\eta\rvert < 2.47$ (excluding $1.37 < \lvert\eta\rvert < 1.52$) $p_T > 25\,\text{GeV}$ and $\lvert\eta\rvert < 4.4$
VBF topology	$N_\ell = 2$ (same flavour, opposite charge), $m_{\ell\ell} \in (81,\, 100)\,\text{GeV}$ $N_{\text{jets}} \geq 2$, $p_T^{j_1} > 85\,\text{GeV}, p_T^{j_2} > 80\,\text{GeV}$ $p_{T,\ell\ell} > 20\,\text{GeV}, p_T^{\text{bal}} < 0.15$ $m_{jj} > 1000\,\text{GeV}, \Delta y_{jj} > 2, \xi_Z < 1$
Signal region	VBF topology $\oplus$ $N_{\text{jets}}^{\text{gap}} = 0$ and $\xi_Z < 0.5$

Table 3.1: Particle-level definition of the event selection

3.2 Monte-Carlo Sample

The feasibility study uses a narrow-width-approximation [7] Monte-Carlo (MC) sample, consisting of two million events generated at leading order with Sherpa 3.0 [8]. The simulated process is:

$$pp \to Z + jj \to \ell^+ + \ell^- + jj \tag{3.1}$$

Additionally, events with an invariant dijet mass m_{jj} below 110 GeV are discarded.

The MC sample is compared to the measurement by the ATLAS collaboration [1], in Fig. 3.1, showing that the MC sample aligns sufficiently well with the data for the purpose of a feasibility study. Furthermore, the estimated cross-section of the MC sample, $\sigma_{\text{EW}}^{\text{MC}} = (37.75 \pm 0.22)\,\text{fb}$, falls well within the uncertainty range of the ATLAS collaboration measurement, which is $\sigma_{\text{EW}} = (37.4 \pm 3.5 \pm 5.5)\,\text{fb}$ [1]. This agreement provides additional validation for the MC sample.

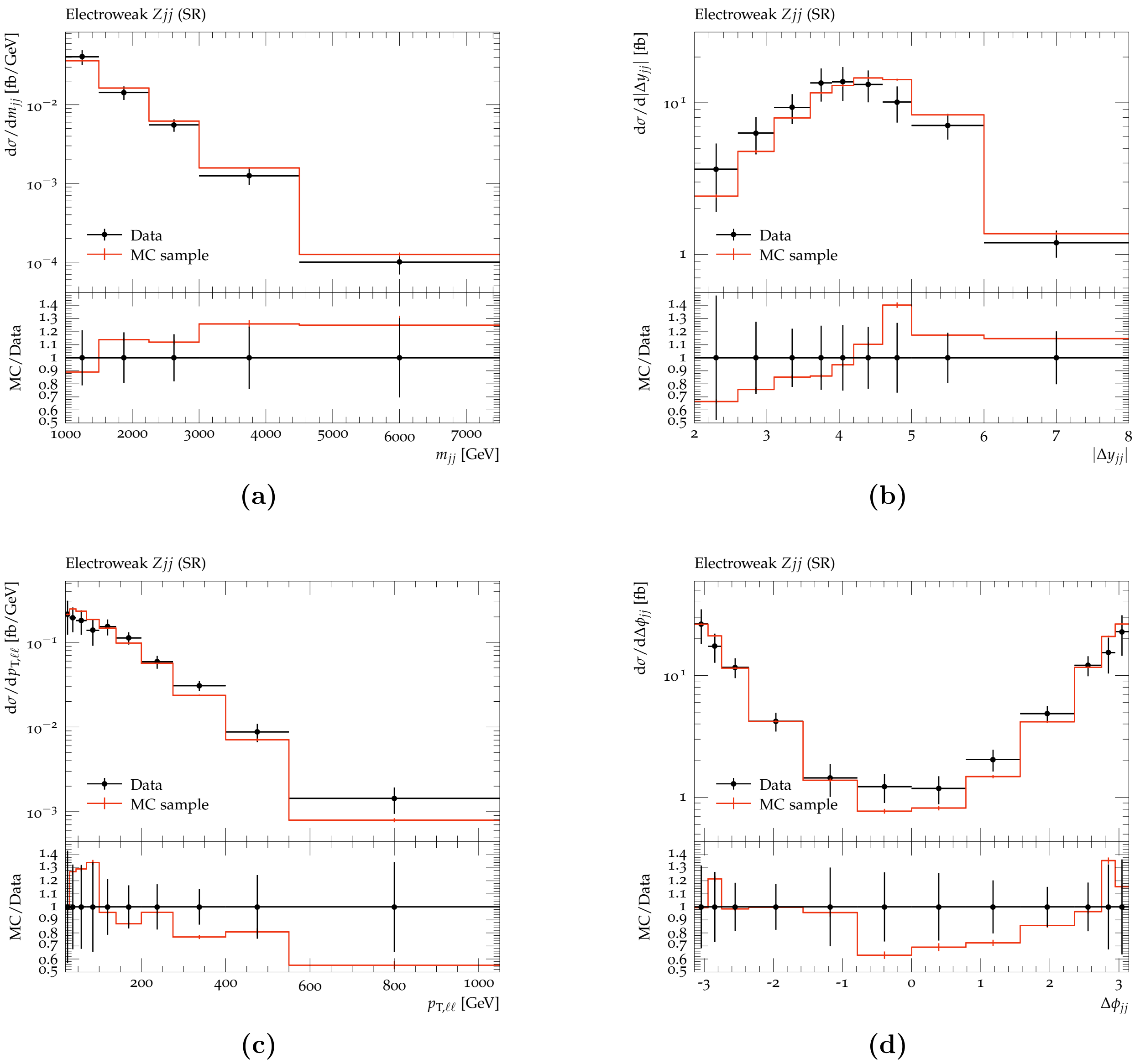

Figure 3.1: Validation of the Monte-Carlo sample via comparison with the ATLAS measurement of the process [1]. The Figure shows the differential cross-section as a function of the invariant dijet mass m_{jj} in a), the rapidity gap between the jets $|\Delta y_{jj}|$ in b), the transverse momentum of the dilepton system $p_{T,\ell\ell}$ in c) and the azimuthal angle gap between the jets $\Delta\phi_{jj}$ in d).

3.3 Method of moments

The first step in the analysis is to determine the angular coefficients A_i that characterize the Z-boson decay distribution in the simulation. Their extraction relies on the orthogonality of the harmonic polynomials P_i. The corresponding angular coefficient can be isolated by taking the weighted average of the angular distribution with respect to any specific polynomial. Formally, the moment of a polynomial $P_i(\cos\theta, \phi)$ over a specific range of p_T^Z, y^Z and m^Z is defined as:

$$\langle P_i(\cos\theta, \phi)\rangle = \frac{\int P_i(\cos\theta, \phi)\, \mathrm{d}\sigma\,(\cos\theta, \phi)\, \mathrm{d}\cos\theta\, \mathrm{d}\phi}{\int \mathrm{d}\sigma\,(\cos\theta, \phi)\, \mathrm{d}\cos\theta\, \mathrm{d}\phi} \tag{3.2}$$

From this definition, explicit relationships between the moments $\langle P_i\rangle$ and the angular coefficients A_i can be derived:

$$\begin{aligned}
\left\langle \frac{1}{2}(1 - 3\cos^2\theta) \right\rangle = \frac{3}{20}\left(A_0 - \frac{2}{3}\right); \quad \langle \sin 2\theta \cos\phi\rangle = \frac{1}{5}A_1; \quad \sin^2\theta\cos 2\phi = \frac{1}{10}A_2 \\
\langle \sin\theta\cos\phi\rangle = \frac{1}{4}A_3; \quad \langle\cos\theta\rangle = \frac{1}{4}A_4; \quad \left\langle \sin^2\theta \sin 2\phi\right\rangle = \frac{1}{5}A_5; \\
\langle \sin 2\theta \sin\phi\rangle = \frac{1}{5}A_6; \quad \langle \sin\theta\sin\phi\rangle = \frac{1}{4}A_7
\end{aligned} \tag{3.3}$$

Because the decomposition of the Z-decay with angular coefficients is only valid in the complete decay phase space, no selection on p_T and η of the leptons is applied at this stage. This explicitly means that the cuts on dressed electrons and dressed muons in Tab. 3.1 are removed. Using the MC sample, the angular coefficients are extracted as follows:

$$\begin{aligned}
A_0 = 1.385, \quad A_1 = -0.012, \quad A_2 = 0.383, \quad A_3 = -0.001, \\
A_4 = -0.004, \quad A_5 = -0.014, \quad A_6 = 0.003, \quad A_7 = 0.012.
\end{aligned} \tag{3.4}$$

The unpolarized cross-section $\frac{\mathrm{d}\sigma^{U+L}}{\mathrm{d}p_T^Z \mathrm{d}y^Z \mathrm{d}m^Z}$ is:

$$\frac{\mathrm{d}\sigma^{U+L}}{\mathrm{d}p_T^Z\, \mathrm{d}y^Z\, \mathrm{d}m^Z} = 61.9\,\mathrm{fb} \tag{3.5}$$

By inserting these values into Eq. 2.2, a closed-form analytical expression for the differential cross-section over the full Z-boson decay phase space is obtained. This analytical representation is validated by comparing it to the MC sample in projections of $\cos\theta$ and ϕ, as shown in Fig. 3.2. While no angular binning is required to extract these coefficients using the method of moments, a binning scheme is introduced for subsequent visualization and further analysis. Specifically, the angular distributions are represented in eight equidistant $\cos\theta$ bins spanning $[-1, 1]$ and eight equidistant ϕ bins covering $[0, 2\pi]$, following the binning choice made in Ref. [2]. This choice of binning allows differential measurements later. It was verified that increasing the number of angular bins does not significantly improve the uncertainties of the studies presented in Chapter 4. Therefore, this binning strategy is sufficient for the purpose of this analysis.

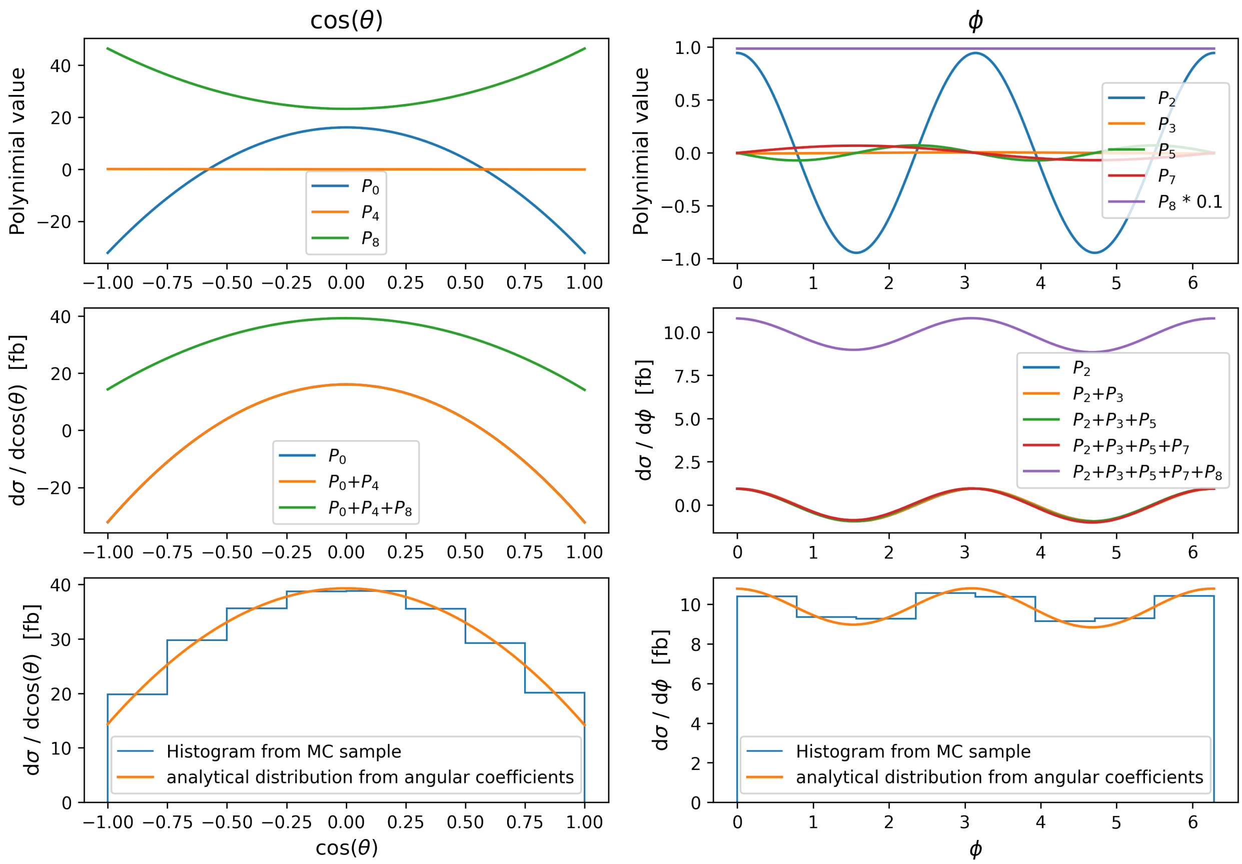

Figure 3.2: Validation for the decomposition with angular coefficients. The polynomials that vanish in the projections of the angular decomposition (see Eq. 2.4 and Eq. 2.5) are not shown.

3.4 Methodology to build templates

Since the angular decomposition is only valid in the complete phase space of the Z-boson decay, the analytical form of the harmonic polynomials in the presence of selections on the lepton kinematics is unknown. To find the corresponding shape of the harmonic polynomials in the presence of these selections, templates are constructed by reweighting the MC events with a methodology used by the ATLAS collaboration [2], which is to be explained in the following.

Since the analytical form of the angular distribution before applying cuts on lepton kinematics is already known with the extracted angular coefficients, it can be used to modify the

MC events in a controlled way. First, the weight of each MC event is divided by its predicted angular distribution value. This procedure “flattens” the angular distribution across the entire decay phase space, effectively erasing any initial polarization imprint and resulting in a uniform angular spectrum. With a flat distribution in hand, the shape of each polynomial P_i is recovered by multiplying the event weight with the value of the polynomial itself on an event-by-event basis – initially without lepton-level cuts. Finally, reintroducing the cuts directly incorporates the selection efficiencies' shape effects into the templates.

Performing this procedure for all nine harmonic polynomials generates nine distinct template histograms. By construction, these templates represent the polynomials in the presence of a selection on lepton kinematics. Summing these templates exactly reproduces the angular distribution observed in the MC sample, forming a robust “pseudo-analytical” model of the angular dependence within the selected phase space. Figure 3.3 illustrates the projections of the templates on $\cos\theta$ and ϕ before applying the lepton-level cuts. These projections closely match the expected shapes from Eq. 2.4 and Eq. 2.5, confirming the internal consistency of the method. The templates derived with the full selection on the lepton kinematics are shown in Figure 3.4. In comparison with the baseline templates, deviations from the theoretical curves show the shape effects of the selection that are incorporated into the templates.

Additionally, as anticipated, polynomials that are expected to vanish in specific projections remain negligible. Altogether, these checks validate the methodology and the resulting templates. Templates built in the presence of the selections on lepton kinematics will be referred to as templates with lepton cuts, while templates built in their absence will be referred to as templates without lepton cuts.

3.5 Summary

In summary, the angular coefficients are first extracted from the Monte Carlo sample by taking moments of each harmonic polynomial in a fully inclusive decay phase space (i.e., without any final-state lepton cuts). With these coefficients in hand, each MC event is then adjusted individually. First, its weight is divided by that specific event's calculated angular distribution value, thereby “flattening” the angular spectrum. Next, still on an event-by-event basis, the weight is multiplied by each polynomial to construct nine distinct template histograms. After applying the full selection criteria, the templates naturally incorporate the effects of selection efficiencies. In this way, the resulting templates serve as practical pseudo-analytical functional forms of the harmonic polynomials within the final, cut-applied analysis phase space.

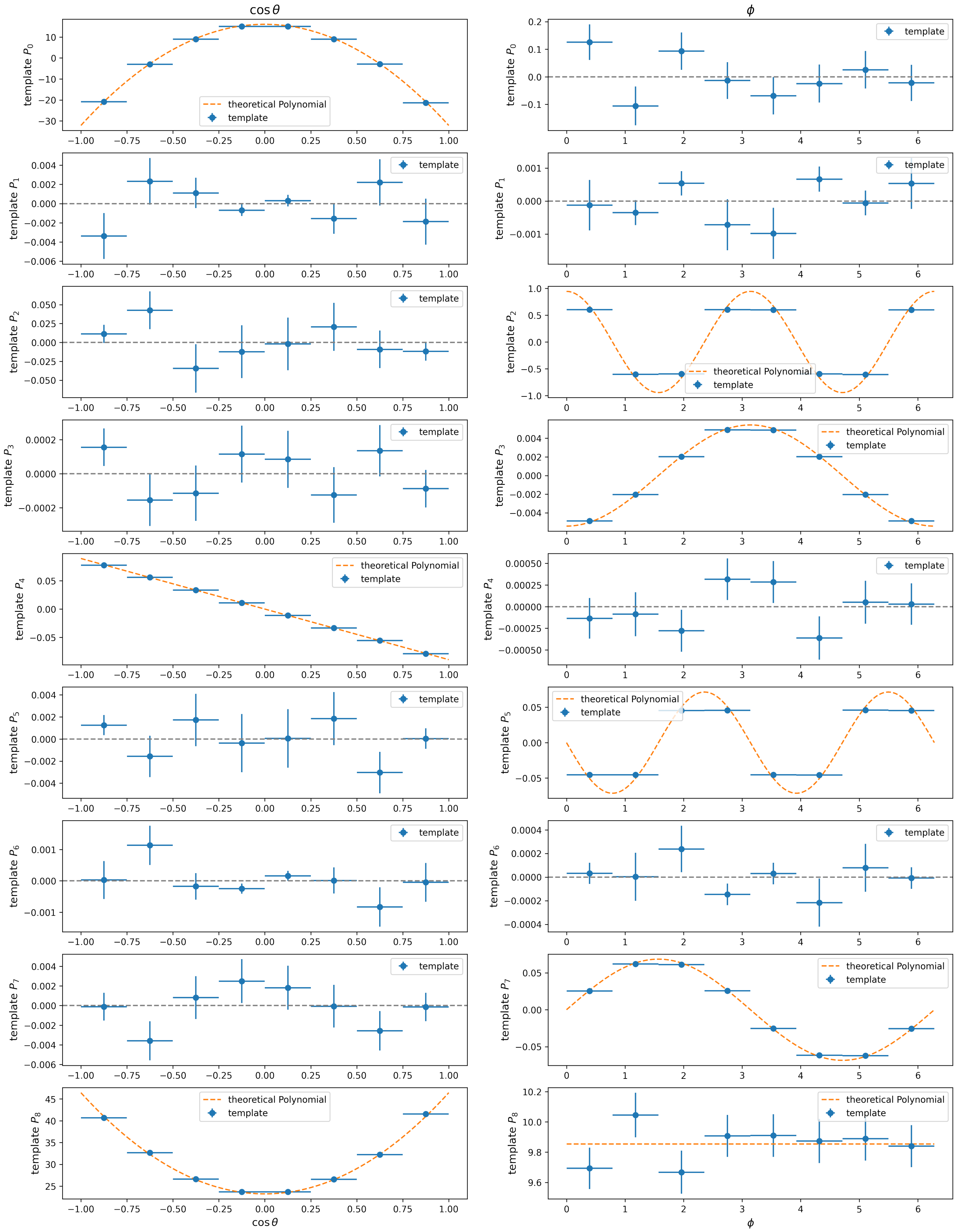

Figure 3.3: Projections of templates without lepton cuts compared with theoretical angular distribution from Eq. 2.4 and 2.5 respectively

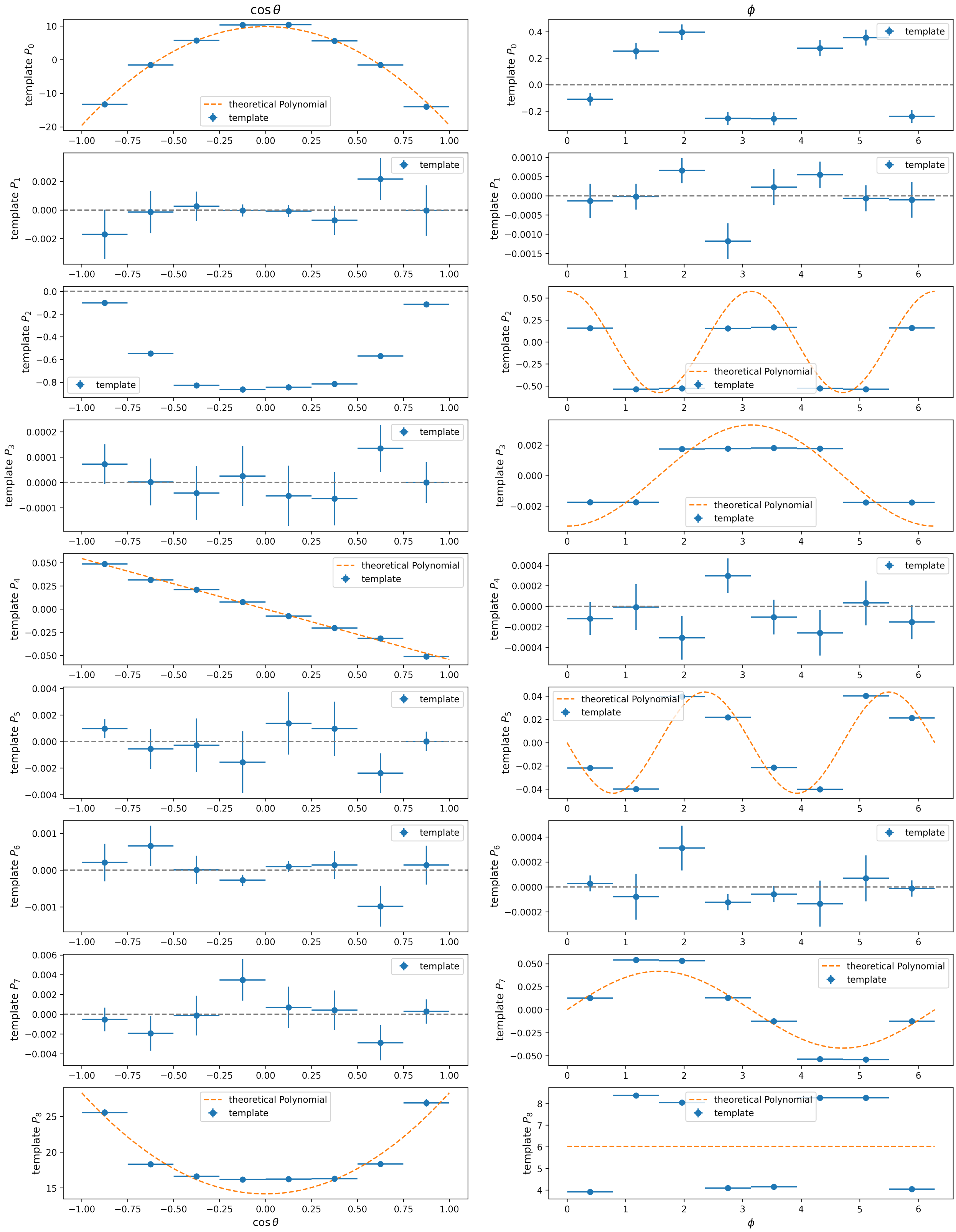

Figure 3.4: Projections of templates with lepton cuts compared with theoretical angular distribution from Eq. 2.4 and 2.5 respectively

4 Results

In the previous chapter, templates were constructed as pseudo-analytical representations of the harmonic polynomials when lepton kinematic selections are included. This chapter aims to evaluate the feasibility of measuring the longitudinal polarization fraction using data. For this purpose, the MC sample is scaled to an integrated luminosity of $140\,\mathrm{fb}^{-1}$ and treated as pseudo-data. This luminosity corresponds to the total data collected during LHC Run 2, making it a realistic benchmark for this feasibility study. The longitudinal polarization fraction is determined by fitting the templates to the pseudo-data to extract the angular coefficients, mainly focusing on A_0, which is used to calculate the polarization via Eq. 2.3. Additionally, the feasibility of performing this measurement differentially as a function of p_T^Z is explored.

The chapter is structured as follows: First, the fitting methodology is introduced, outlining the approach used to estimate the angular coefficients and their uncertainties. This is followed by initial tests performed inclusively in p_T^Z to validate the accuracy of the fitting procedure. Next, the analysis is extended by introducing binning in p_T^Z to assess the method's feasibility in different kinematic regions. Finally, the longitudinal polarization fraction is calculated, comprehensively evaluating the potential for measuring longitudinal polarization in Zjj events.

4.1 Fitting methodology

To extract the angular coefficients from a dataset, the following functional form is fitted:

$$\lambda_j(\{x_k\}) = x_8 \left(T_{j8} + \sum_{k=0}^{7} x_k \cdot T_{jk}, \right) \tag{4.1}$$

T_{jk} represents the template value corresponding to the angular coefficient A_k in the angular bin j, and x_k are normalization parameters for each template with respect to the general normalization x_8. This function returns the number of expected events $\lambda_j(\{x_k\})$ for a given set of parameters $\{x_k\}$ in bin the angular bin j. To measure the parameters x_k, a Poisson likelihood $\mathcal{L}$ is maximized by minimizing $-\ln\mathcal{L}$ using the Migrad minimizer from iMinuit [9]:

$$\begin{aligned} -\ln\mathcal{L} &= -\sum_j \ln P_j(k_j|\lambda_j) \\ \text{with } \ln P_j(k_j|\lambda_j) &= \ln\left(\frac{\lambda_j^{k_j} e^{-\lambda_j}}{k_j!}\right) = k_j \ln\lambda_j - \lambda_j + \text{const.} \end{aligned} \tag{4.2}$$

Here, k_j represents the observed number of events in bin j.

Since the same MC sample used to construct the templates is also employed as pseudo-data for the fitting procedures, these fits act as closure tests to verify the correctness of the fitting methodology. While the uncertainties correspond to an estimate of the statistical uncertainties of a measurement in data, albeit not accounting for the effects of background contributions and detector effects. To ensure the expected value of the normalization parameters is 1.0, the templates are scaled to match the integrated luminosity of the pseudo-data.

4.2 Feasibility study of a measurement in the fiducial phase space

4.2.1 Fitting with templates projected on the $\cos\theta$ axis

As an initial test, the fit is performed in projections of the distributions on the $\cos\theta$ axis, allowing the extraction of the coefficients A_0, A_4, and A_8. In these fits, the normalization of the templates of the remaining coefficients, whose harmonic polynomials vanish in the $\cos\theta$ projection, are fixed to their theoretical value of 1.0.

Name	Value	Hesse Error
x0	1.000	0.022
x4	1	6
x8	1.000	0.011

Table 4.1: Normalisation parameters for the templates obtained in a fit to pseudo-data. The fit was performed in the projection of the data on the $\cos\theta$ axis in the fiducial phase space without any selections on the leptons applied.

As shown in Tab. 4.1, the parameters align with their expected value when fitting the templates without lepton cuts. This closure test demonstrates that the templates reproduce the analytical form in Eq. 2.5. When comparing this to the fit of the projected templates with lepton cuts, shown in Fig. 4.1 and Tab. 4.2, the uncertainties increase slightly due to the reduction in statistics. Nevertheless, the uncertainty on A_0, the key parameter for determining the longitudinal polarization fraction, remains low at approximately 3 %.

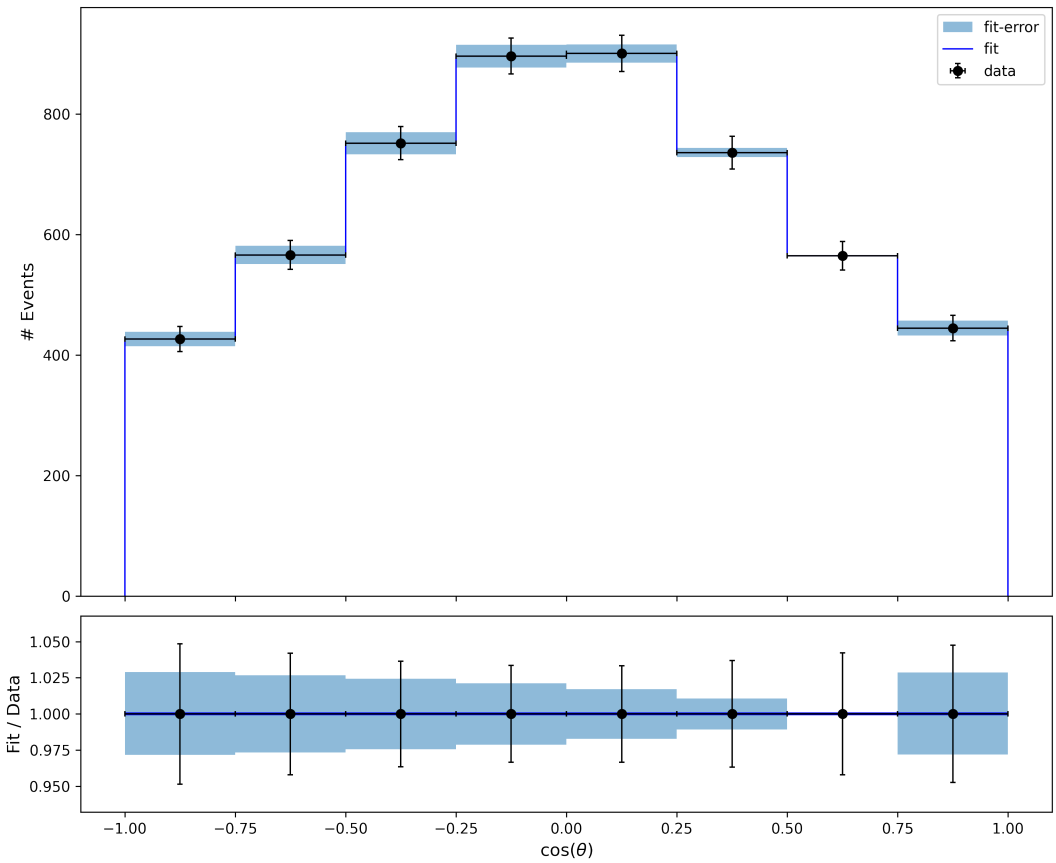

Figure 4.1: Fit of the templates to pseudo-data. The fit was performed in the projection of the data on the $\cos\theta$ axis in the fiducial phase space with a selection on the leptons applied.

Name	**Value**	**Hesse Error**
x0	1.000	0.026
x4	1	7
x8	1.000	0.014

Table 4.2: Normalisation parameters for the templates obtained in a fit to pseudo-data. The fit was performed in the projection of the data on the $\cos\theta$ axis in the fiducial phase space with a selection on the leptons applied.

4.2.2 Fitting with double differential templates

Having validated the fitting procedure with the $\cos\theta$ projection, the analysis is now extended to the double differential templates with lepton cuts to extract all angular coefficients. The uncertainty on A_0, shown in Tab. 4.3, does not significantly increase compared to the projected template fit despite the additional degrees of freedom. The results show sensitivity primarily to A_0, A_2, and A_8. These coefficients are all positively correlated, as seen in Tab. 4.4.

Name	Value	Hesse Error
x0	1.000	0.027
x1	1.0	3.5
x2	1.00	0.27
x3	0	40
x4	1	7
x5	1.0	2.6
x6	1	10
x7	1.0	2.4
x8	1.000	0.016

Table 4.3: Normalisation parameters for the templates obtained in a fit to pseudo-data. The fit was performed with the double differential templates in the fiducial phase space with a selection on the leptons applied.

	x0	**x1**	**x2**	**x3**	**x4**	**x5**	**x6**	**x7**	**x8**
x0	0.000717	-0.9e-3 (-0.010)	1.5e-3 (0.203)	6.6e-3 (0.006)	-4.6e-3 (-0.024)	0.2e-3 (0.004)	0.3e-3	-0.4e-3 (-0.006)	0.04e-3 (0.092)
x1	-0.9e-3 (-0.010)	12.4	0.01	-0 (-0.001)	0 (0.010)	0 (0.006)	0 (0.004)	0 (0.003)	0.22e-3 (0.004)
x2	1.5e-3 (0.203)	0.01	0.0745	-0.05 (-0.004)	-0.01 (-0.005)	0.00 (0.004)	0.01 (0.004)	-0.00 (-0.006)	2.30e-3 (0.522)
x3	6.6e-3 (0.006)	-0 (-0.001)	-0.05 (-0.004)	1.94e+03	-0 (-0.005)	0 (0.004)	0 (0.003)	1 (0.006)	-2.73e-3 (-0.004)
x4	-4.6e-3 (-0.024)	0 (0.010)	-0.01 (-0.005)	-0 (-0.005)	50.1	-0 (-0.003)	-0 (-0.013)	-0 (-0.001)	0.38e-3 (0.003)
x5	0.2e-3 (0.004)	0 (0.006)	0.00 (0.004)	0 (0.004)	-0 (-0.003)	6.75	-0 (-0.003)	0 (0.003)	0.16e-3 (0.004)
x6	0.3e-3	0 (0.004)	0.01 (0.004)	0 (0.003)	-0 (-0.013)	-0 (-0.003)	101	-0 (-0.005)	0.29e-3 (0.002)
x7	-0.4e-3 (-0.006)	0 (0.003)	-0.00 (-0.006)	1 (0.006)	-0 (-0.001)	0 (0.003)	-0 (-0.005)	5.65	-0.09e-3 (-0.002)
x8	0.04e-3 (0.092)	0.22e-3 (0.004)	2.30e-3 (0.522)	-2.73e-3 (-0.004)	0.38e-3 (0.003)	0.16e-3 (0.004)	0.29e-3 (0.002)	-0.09e-3 (-0.002)	0.00026

Table 4.4: The covariance matrix for the normalization parameters of the double differential templates with lepton cuts, shown in Tab. 4.3. The Pearson correlation coefficient is shown in brackets behind the covariance value

4.2.3 Summary

When fitting the double differential templates, all parameters can be extracted in theory. However, because the polynomials P_0, P_2, and P_8 dominate the angular distribution, the corresponding coefficients are the ones to which the fits are most sensitive. However, A_0 is enough to calculate the longitudinal polarization with Eq. 2.3. Since fitting all parameters in the double differential fit does not significantly increase the overall fit uncertainties compared to fitting a subset of the parameters in projections of the templates, the differential analysis in p_T^Z bins is done using the double differential template fits.

4.3 Feasibility study of a differential measurement in p_T^Z

To evaluate the feasibility of measuring angular coefficients differentially in p_T^Z, the template-building methodology described in the previous chapter is applied separately within each p_T^Z bin, yielding a set of nine templates for each p_T^Z bin. To optimize the binning, the angular coefficient A_0 uncertainty is used as a benchmark, as A_0 is directly related to the longitudinal polarization fraction of the Z-boson f_L^Z. The optimization process starts from an equidistant 5 GeV binning between 20 GeV and 200 GeV, and an equidistant 25 GeV binning between 200 GeV and 400 GeV. It then proceeds at the highest p_T^Z bin and iteratively merges adjacent bins until the A_0 uncertainty falls below 10 %. At low p_T^Z values, a problem arises due to low selection efficiency for events where $\cos\theta$ is near ± 1. In the case of angular bins that do not contain any events for low p_T^Z, the $\cos\theta$ binning scheme is adjusted to have the following bin boundaries:

$$\cos\theta_{\text{bin boundaries}} : \{-1, -0.5, -0.25, 0, 0.25, 0.5, 1\} \tag{4.3}$$

ensuring that all angular bins contain at least one event.

After applying the binning optimization procedure, the final p_T^Z binning scheme consists of seven bins:

$$p^Z_{T,\text{bin bounderies}} : \{20.0,\ 60.0,\ 85.0,\ 100.0,\ 120.0,\ 145.0,\ 190.0,\ 400.0\} \tag{4.4}$$

The values of the angular coefficients are calculated from the estimated normalisation parameters by dividing the corresponding templates by their analytical value A_k.

$$\lambda_j(\{x_k\}) = \frac{x_8}{\frac{\mathrm{d}\sigma^{U+L}}{\mathrm{d}p_T^Z}} \left(T_{j8} + \sum_{k=0}^{7} \frac{x_k}{A_{k,\text{analytical}}} T_{jk} \right) \tag{4.5}$$

The fit result for the angular coefficients is shown in Fig. 4.2 and indicates that the analysis is primarily sensitive to A_0. Using the extracted values of A_0, the fractional longitudinal polarization f_L^Z is calculated with Eq. 2.3 and displayed in Fig. 4.3. The results show that it is possible to measure the longitudinal polarization fraction differentially in seven p_T^Z bins reaching 400 GeV with a statistical uncertainty below the set goal of 10 %.

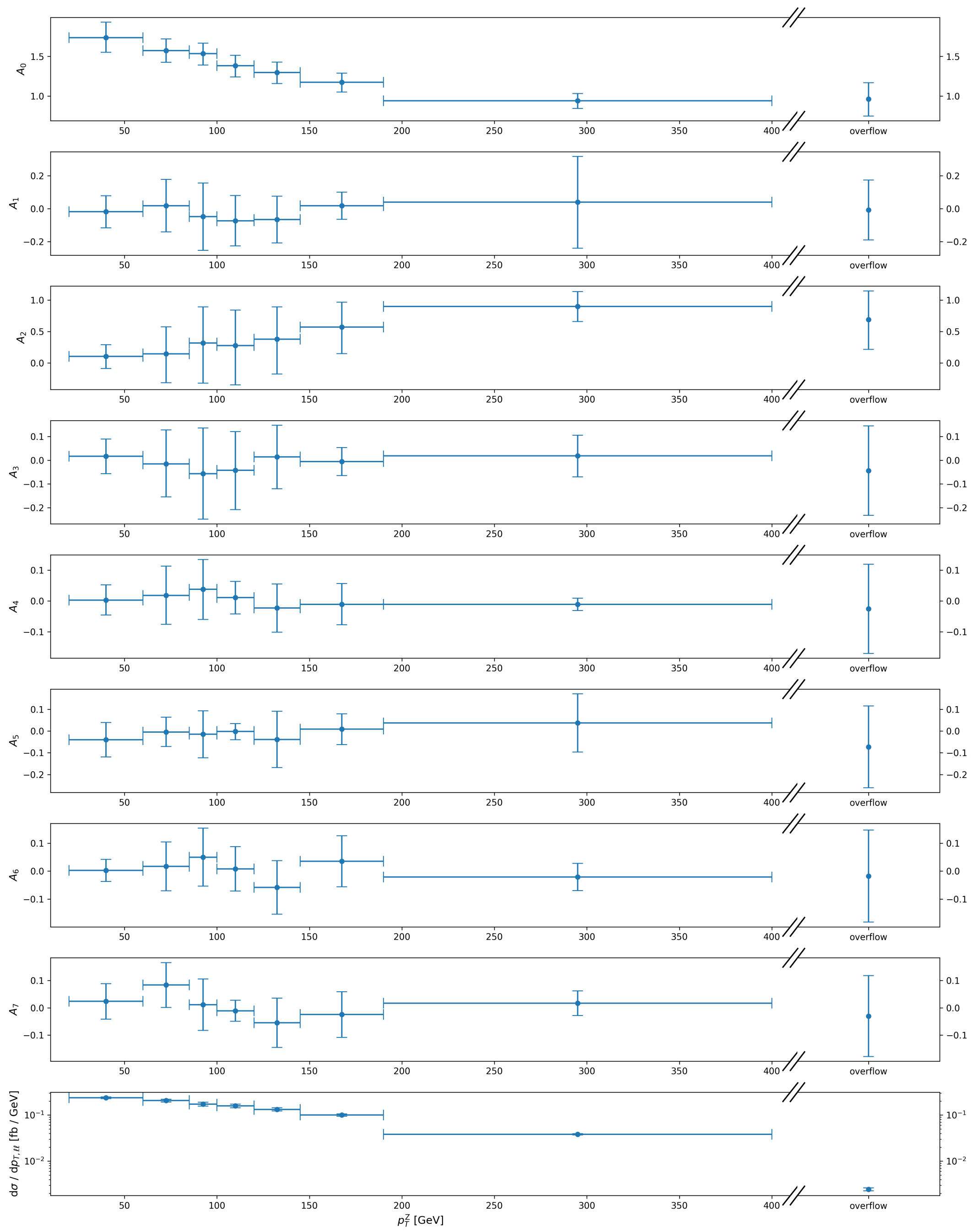

Figure 4.2: Fitting result for the p_T^Z binned fits of the full templates. The bin optimization in p_T^Z yields seven bins with the binedges: $\{20.0, 60.0, 85.0, 100.0, 120.0, 145.0, 190.0, 400.0\}$

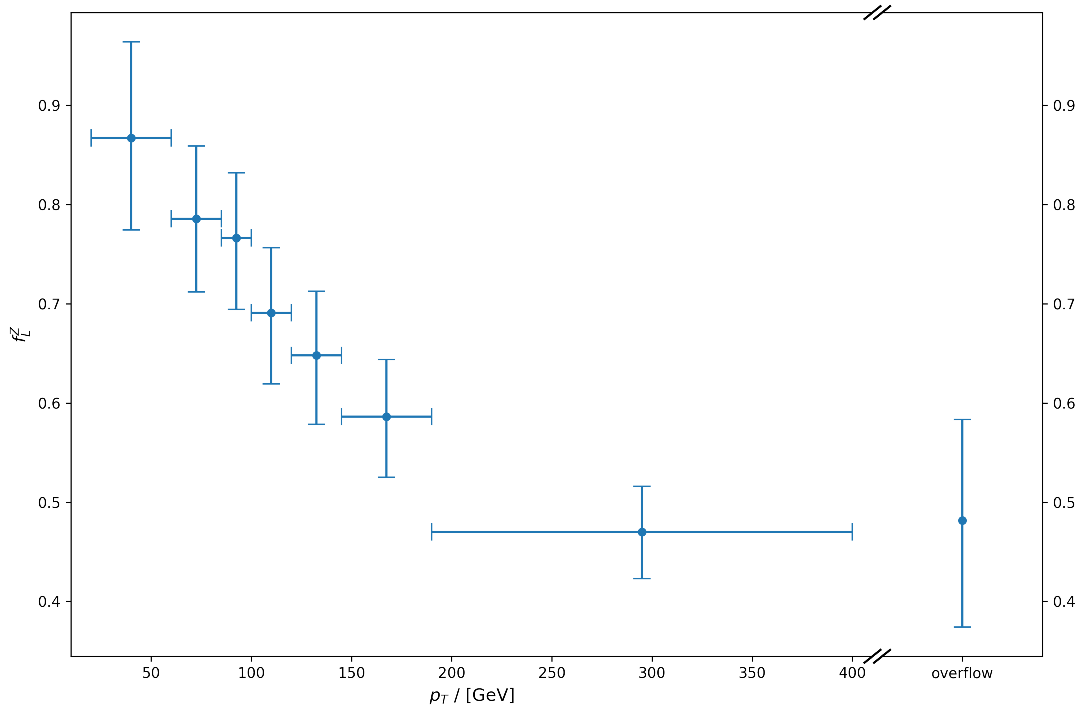

Figure 4.3: Longitudinal polarization of the Z-boson calculated with Eq. 2.3

5 Conclusion

The longitudinal polarization states of the electroweak gauge bosons provide rich insights into the structure of the electroweak theory. This thesis explored the feasibility of polarization measurements in processes called vector-boson fusion. In the fiducial phase space of a previous measurement [1] of electroweak Zjj production, the method of moments was employed to extract the angular coefficients from simulation analytically. However, since the angular decomposition is invalid in the presence of lepton kinematic selections, this approach cannot be directly applied to data. To address this, templates were constructed to represent the harmonic polynomials while incorporating these kinematic selections. Closure tests confirmed the effectiveness of this approach, demonstrating that the developed fitting methodology successfully extracts the angular coefficients through double-differential fits. The analysis showed sensitivity primarily to the coefficients $A_0,\ A_2,$ and A_8, which dominate the angular distribution.

To explore the possibility of differential measurements of polarization, the longitudinal polarization fraction was studied as a function of the transverse momentum of the Z-boson. An optimization study showed that a measurement can achieve a precision of better than $10\,\%$ in seven bins with a $p_T^Z < 400\,\mathrm{GeV}$. In this exploratory analysis, the statistical uncertainty on the differential cross-section measurement in the fiducial phase space is $1.6\,\%$, which is significantly smaller than the $9.4\,\%$ uncertainty in the corresponding ATLAS measurement [1]. This optimistic estimate arises because this analysis does not incorporate detector inefficiencies that increase the statistical uncertainties in a measurement in data. Furthermore, the large background from strong Zjj production can significantly increase the statistical uncertainties. Nevertheless, by the summer of 2026, $250\,\mathrm{fb}^{-1}$ of pp collision data at $\sqrt{s} = 13.6\,\mathrm{TeV}$ is expected to be collected, and this larger data set will partially compensate this discrepancy. The methodology employed in this thesis and the techniques developed for optimizing the differential measurements are promising avenues for future measurements of the polarization of the Z-boson produced in vector-boson fusion in this dataset.

Appendix

1 Polynom shape for different p_T^Z bins

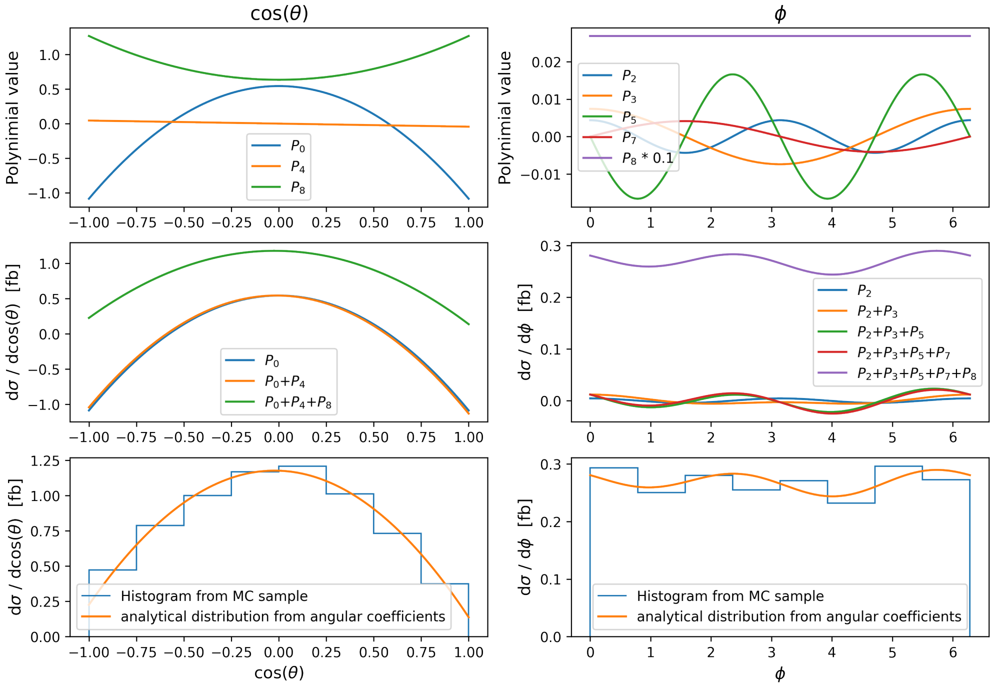

Figure 5.1: Shapes of the polynoms in p_T^Z-bin [30.0, 35.0] GeV

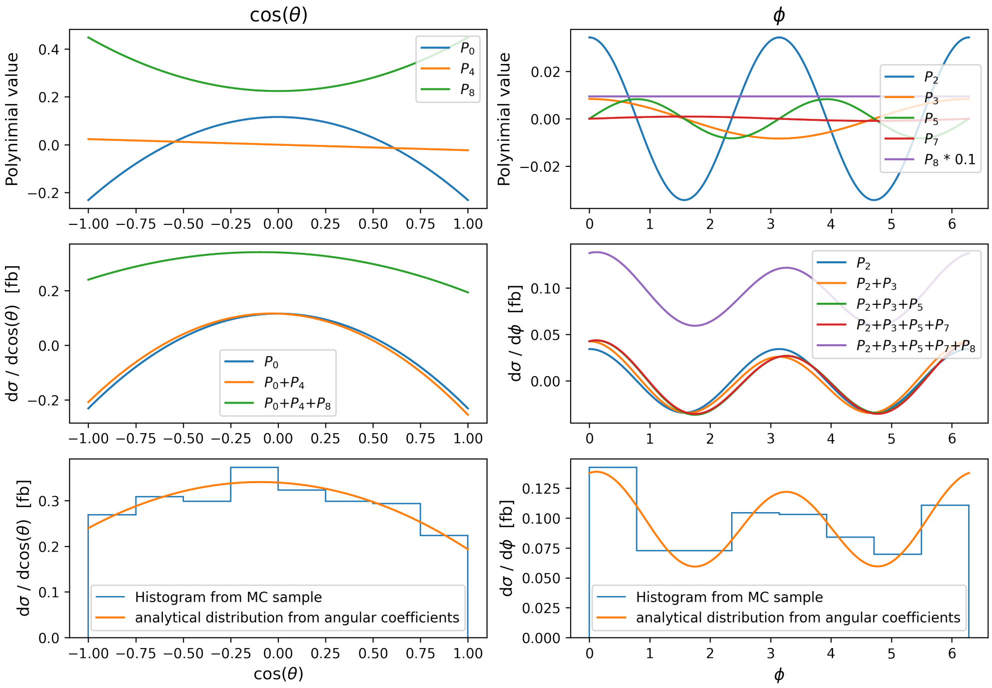

Figure 5.2: Shapes of the polynoms in p_T^Z-bin [195.0, 200.0] GeV

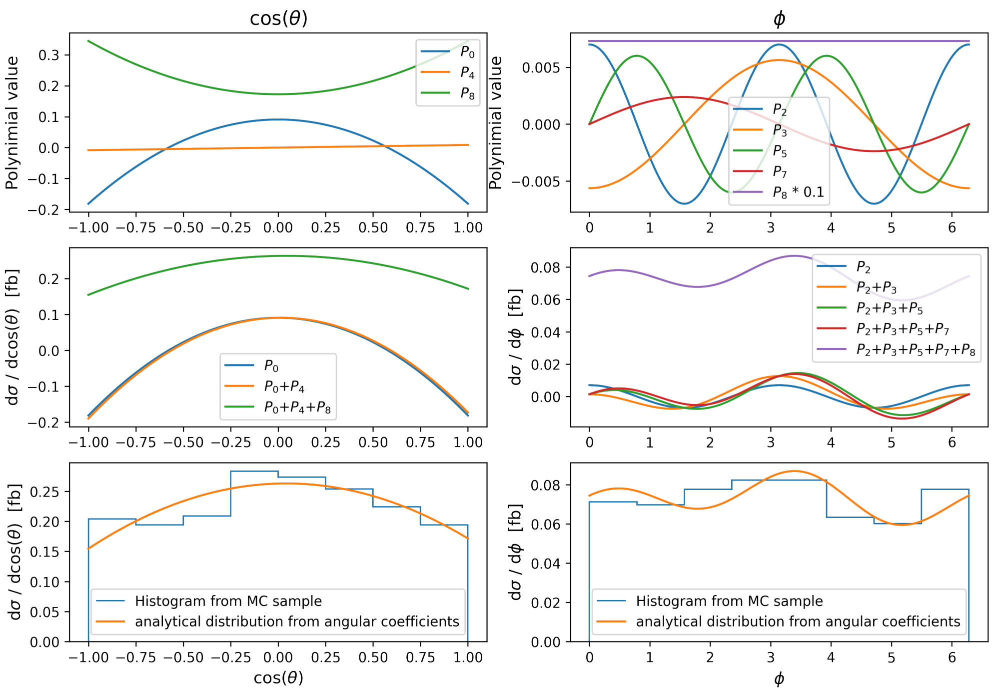

Figure 5.3: Shapes of the polynoms in p_T^Z-bin [375.0, 400.0] GeV

2 Templates in p_T^Z bins

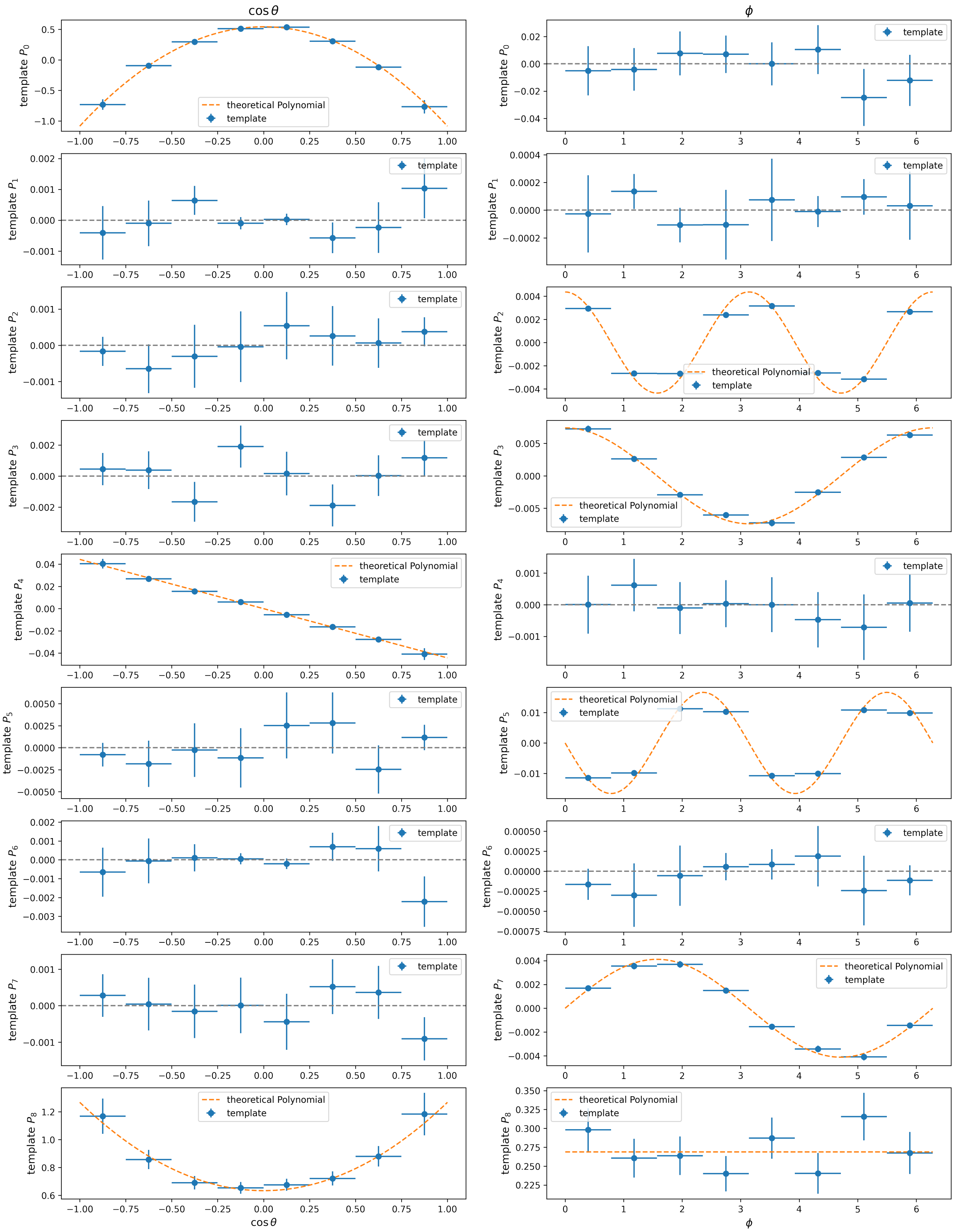

Figure 5.4: Projections of templates without lepton cuts compared with theoretical angular distribution from Eq. 2.4 and 2.5 respectively in p_T^Z-bin [30.0, 35.0] GeV

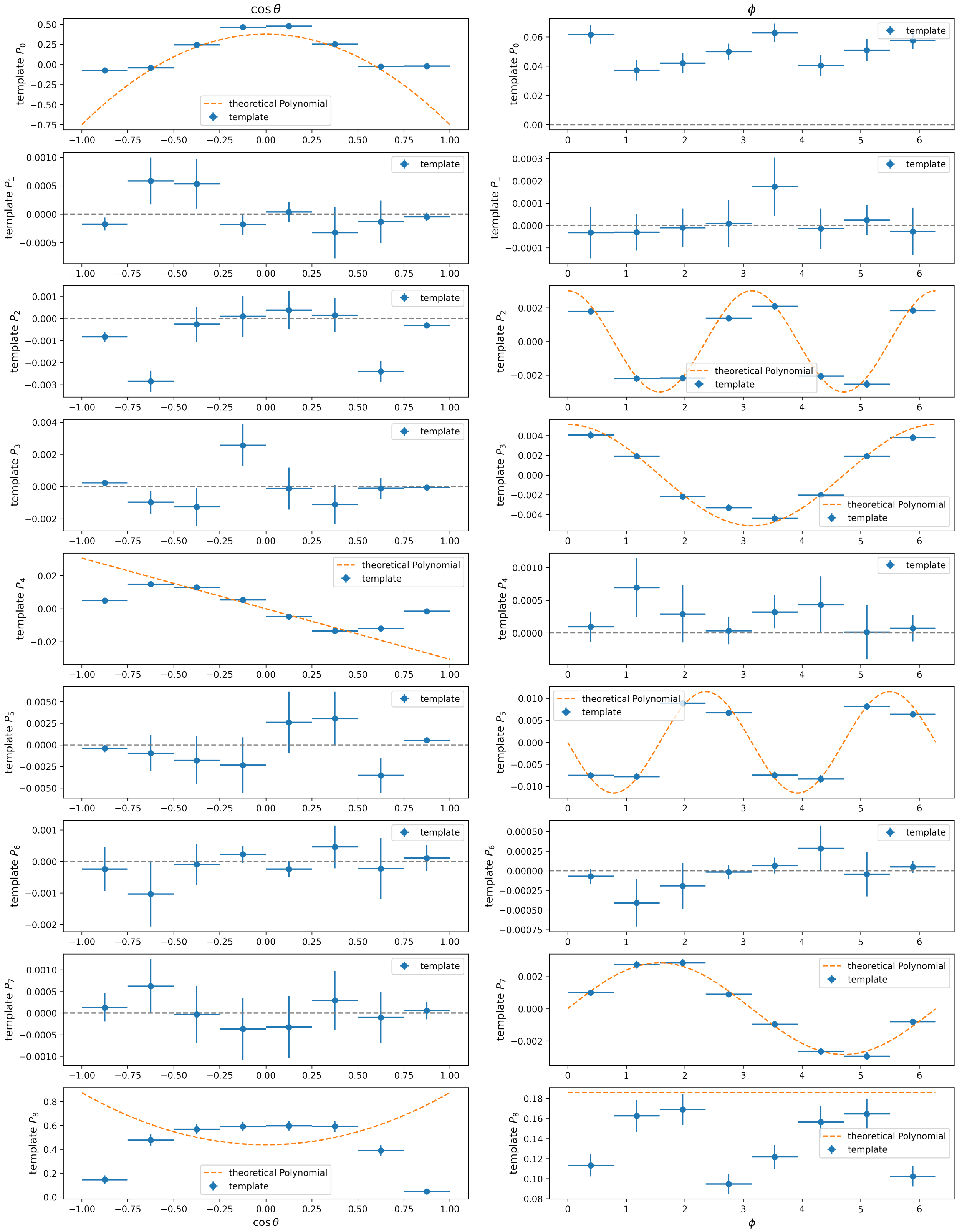

Figure 5.5: Projections of templates with lepton cuts compared with theoretical angular distribution from Eq. 2.4 and 2.5 respectively in p_T^Z-bin [30.0, 35.0] GeV

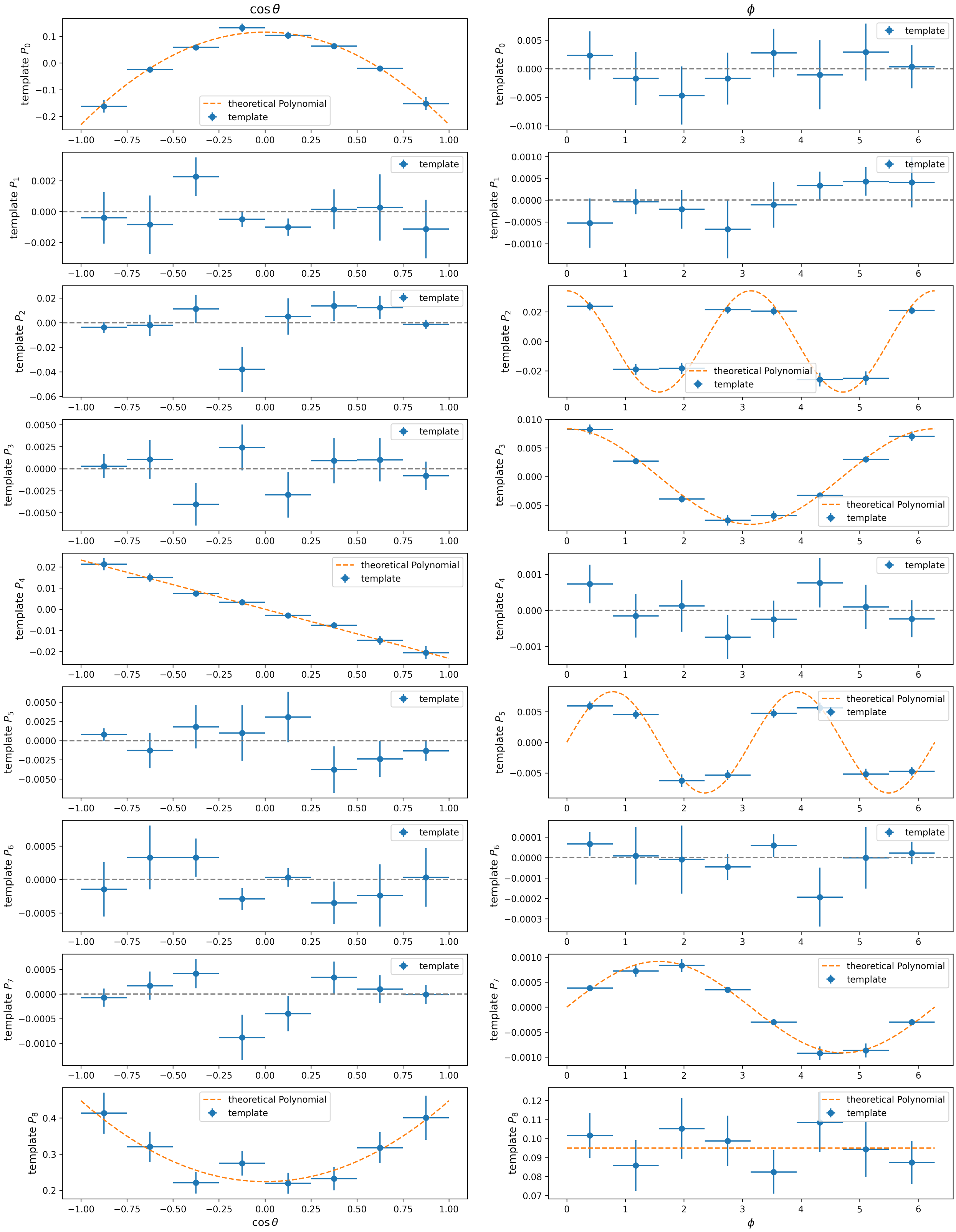

Figure 5.6: Projections of templates without lepton cuts compared with theoretical angular distribution from Eq. 2.4 and 2.5 respectively in p_T^Z-bin [195.0, 200.0] GeV

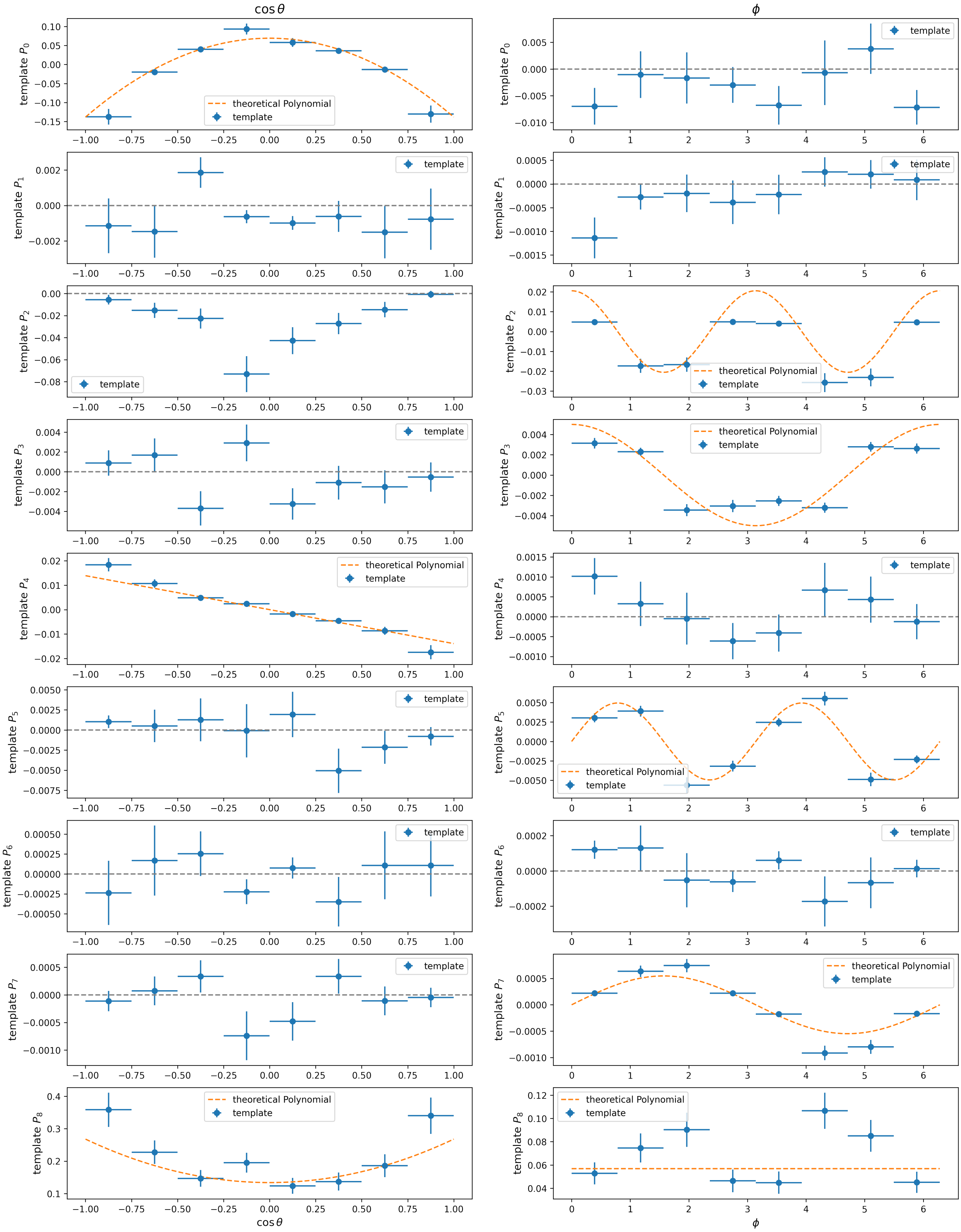

Figure 5.7: Projections of templates with lepton cuts compared with theoretical angular distribution from Eq. 2.4 and 2.5 respectively in p_T^Z-bin [195.0, 200.0] GeV

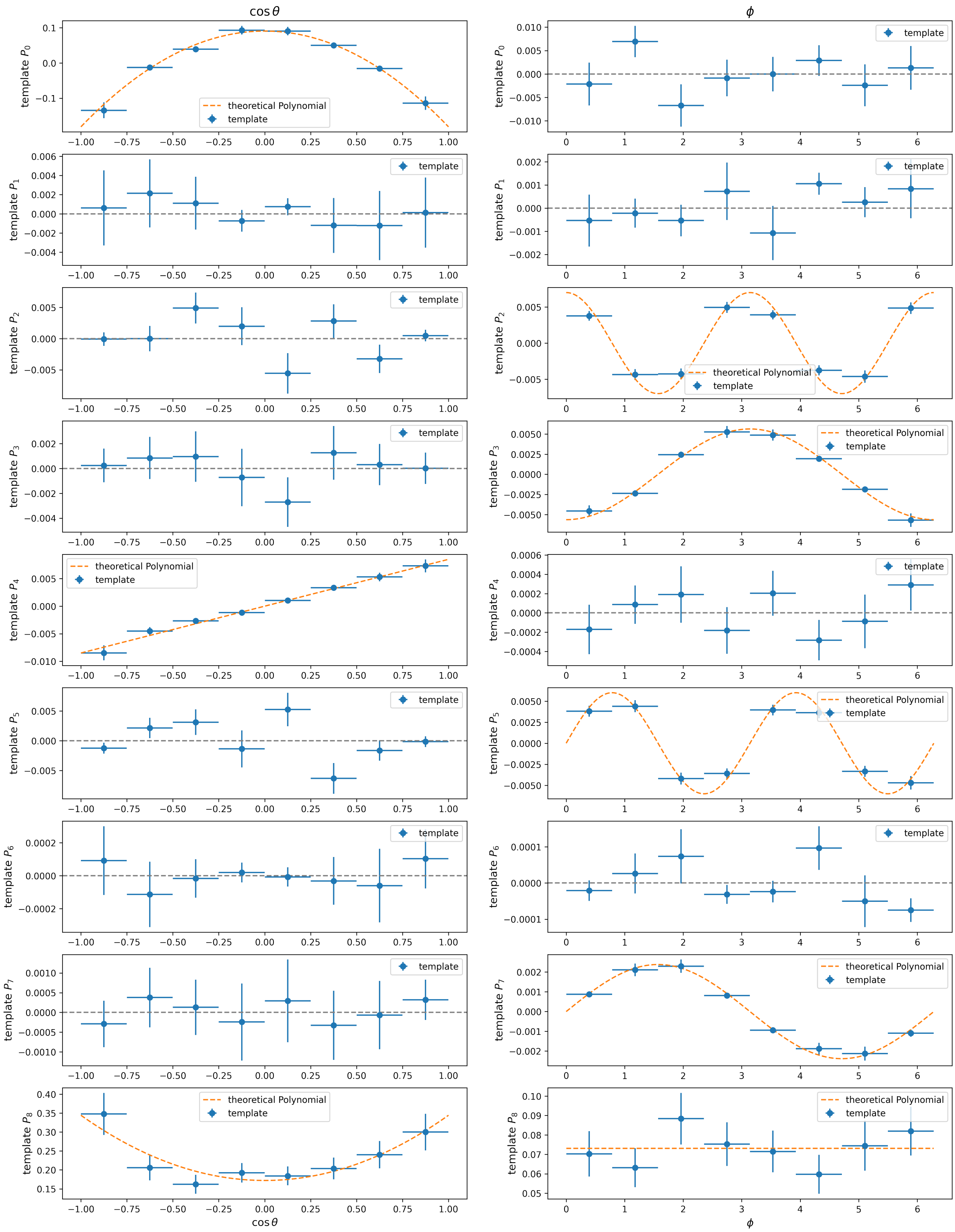

Figure 5.8: Projections of templates without lepton cuts compared with theoretical angular distribution from Eq. 2.4 and 2.5 respectively in p_T^Z-bin [375.0, 400.0] GeV

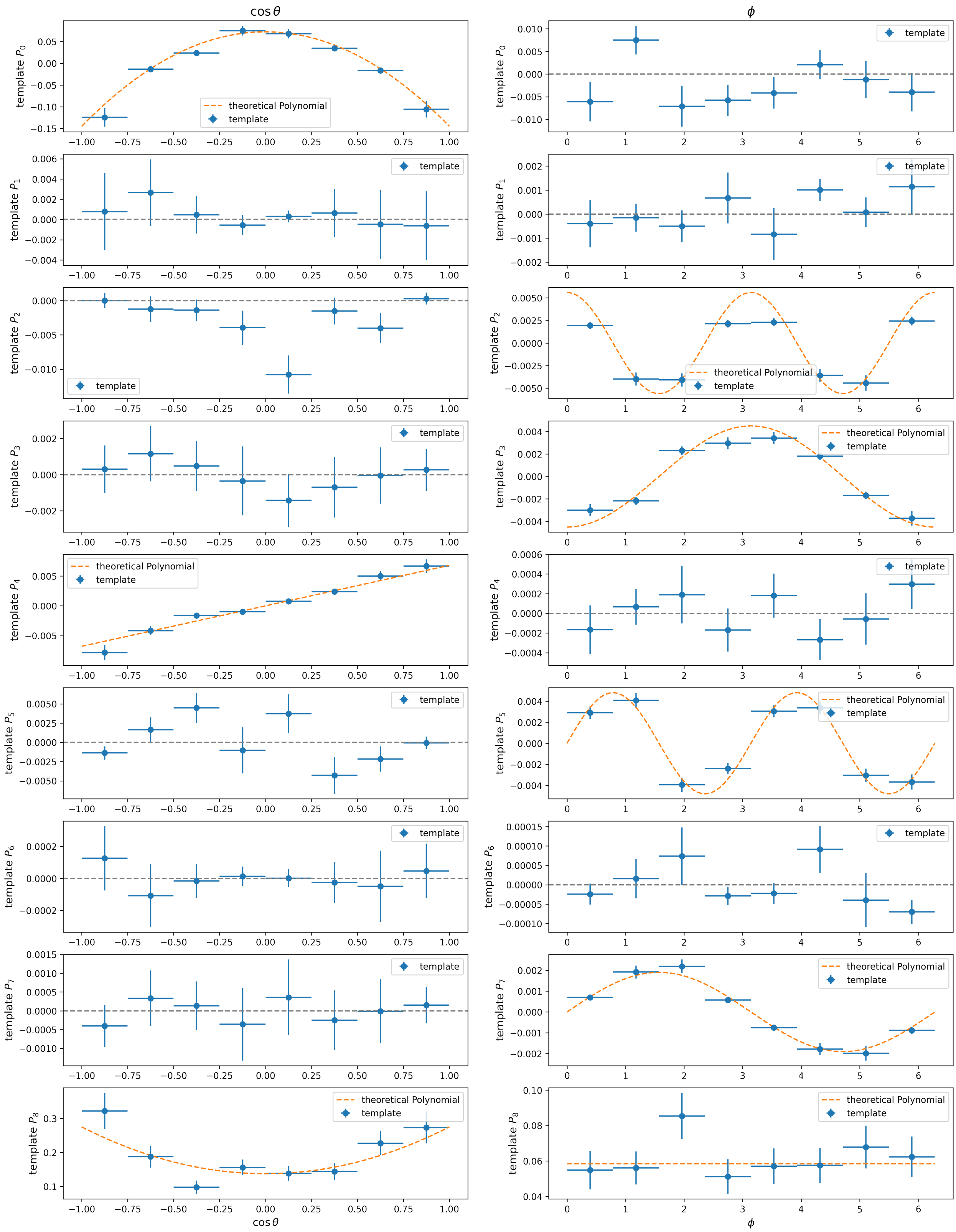

Figure 5.9: Projections of templates with lepton cuts compared with theoretical angular distribution from Eq. 2.4 and 2.5 respectively in p_T^Z-bin [375.0, 400.0] GeV

Bibliography

[1]G. Aad et al., "Measurement of the angular coefficients in Z-boson events using electron and muon pairs from data taken at $\sqrt{s} = 8$ TeV with the ATLAS detector", JHEP **08**, 159 (2016) 10.1007/JHEP08(2016)159, arXiv:1606.00689 [hep-ex].

[2]G. Aad et al., "Differential cross-section measurements for the electroweak production of dijets in association with a Z boson in proton–proton collisions at ATLAS", Eur. Phys. J. C **81**, 163 (2021) 10.1140/epjc/s10052-020-08734-w, arXiv:2006.15458 [hep-ex].

[3]W. Commons, *Standard model illustration*, (2024) https://en.wikipedia.org/wiki/File:Standard_Model_of_Elementary_Particles.svg.

[4]M. A. Thomson, *Electroweak unification and the w and z bosons*, Lecture notes for Part III Particle Physics, Michaelmas Term 2011, University of Cambridge, 2011, https://www.hep.phy.cam.ac.uk/~thomson/partIIIparticles/handouts/Handout_13_2011.pdf.

[5]E. Mirkes, "Angular decay distribution of leptons from w-bosons at nlo in hadronic collisions", Nuclear Physics B **387**, 3–85 (1992) https://doi.org/10.1016/0550-3213(92)90046-E, https://www.sciencedirect.com/science/article/pii/055032139290046E.

[6]C. Bierlich et al., "Robust independent validation of experiment and theory: rivet version 3", SciPost Physics **8** (2020) 10.21468/scipostphys.8.2.026, http://dx.doi.org/10.21468/SciPostPhys.8.2.026.

[7]S. Höche et al., "Beyond standard model calculations with sherpa", The European Physical Journal C **75** (2015) 10.1140/epjc/s10052-015-3338-4, http://dx.doi.org/10.1140/epjc/s10052-015-3338-4.

[8]E. Bothmann et al., *Event generation with sherpa 3*, 2024, arXiv:2410.22148 [hep-ph], https://arxiv.org/abs/2410.22148.

[9]H. Dembinski et al., *Scikit-hep/iminuit*, version v2.30.2, Oct. 2024, 10.5281/zenodo.13923658, https://doi.org/10.5281/zenodo.13923658.

[10]D. L. Rainwater, R. Szalapski, and D. Zeppenfeld, "Probing color singlet exchange in $Z +$ two jet events at the CERN LHC", Phys. Rev. D **54**, 6680–6689 (1996) 10.1103/PhysRevD.54.6680, arXiv:hep-ph/9605444.

[11]R. Gauld et al., "Precise predictions for the angular coefficients in z-boson production at the lhc", Journal of High Energy Physics **2017** (2017) 10.1007/JHEP11(2017)003.

[12]M. Müller, *Extracting-angular-coefficients*, Version 1.0, 2024, https://github.com/maml087d/Extracting-angular-coefficients.

[13]M. Müller, *template-fitting*, Version 1.0, 2024, https://github.com/maml087d/template-fitting.

Erklärung

Hiermit erkläre ich, dass ich diese Arbeit im Rahmen der Betreuung am Institut für Kern- und Teilchenphysik ohne unzulässige Hilfe Dritter verfasst und alle Quellen als solche gekennzeichnet habe.

Malte Müller
Dresden, Dezember 2024